Imaging biological tissues with electrical conductivity contrast below 1 S m^{-1} by means of magnetoacoustic tomography with magnetic induction

Gang Hu, Xu Li, and Bin He[a)]
Department of Biomedical Engineering, University of Minnesota, Minnesota 55455, USA

(Received 28 June 2010; accepted 17 August 2010; published online 10 September 2010)

Magnetoacoustic tomography with magnetic induction (MAT-MI) is a recently introduced imaging modality for noninvasive electrical impedance imaging, with ultrasound imaging resolution and a contrast reflecting the electrical conductivity properties of tissues. However, previous MAT-MI systems can only image samples that are much more conductive than real human or animal tissues. To image real biological tissue samples, a large-current-carrying coil that can give stronger magnetic stimulations and stronger MAT-MI acoustic signals is employed in this study. The conductivity values of all the tissue samples employed in this study are also directly measured using a well calibrated four-electrode system. The experimental results demonstrated the feasibility to image biological tissues with electrical conductivity contrast below 1.0 S/m using the MAT-MI technique with safe level of electromagnetic energy applied to tissue samples. © *2010 American Institute of Physics*. [doi:10.1063/1.3486685]

Noninvasive electrical impedance imaging methods have been actively investigated for decades because electrical properties of biological tissues are known to be sensitive to physiological and pathological conditions of living systems. These methods include traditional electrical impedance tomography,[1,2] magnetic resonance electrical impedance tomography,[3,4] magnetic induction tomography,[5] magnetoacoustic tomography,[6,7] and Hall effect imaging.[8] Recently, He and co-workers[9–11] proposed a method termed magnetoacoustic tomography with magnetic induction (MAT-MI). In MAT-MI, a pulsed magnetic stimulation is delivered to a conductive object (e.g., soft tissue) to induce eddy current. With the existence of another static magnetic field, acoustic waves generated by Lorentz force can then be detected for reconstructing an image with contrast indicating the electrical conductivity of the object. Relevant experiment results from high salinity gel phantoms or salted tissues have been previously reported.[10,11] The samples used in these studies are, however, much more conductive than real human or animal tissues where conductivity is commonly below 1.0 S/m at MHz ultrasound frequency.[12] In addition, as the MAT-MI signals generated in these systems were quite weak, data averaging over ten thousand times at each scanning location was generally required. In the present study, a large-current-carrying coil is employed to deliver stronger magnetic stimulation in order to induce a large but safe eddy current in real tissue samples. By collecting ultrasound signals with data averaging of less than 200 times, we are able to image biological samples with electrical conductivity contrast below 1.0 S/m.

In MAT-MI experiments, a pulsed magnetic stimulation $\mathbf{B}_1(\mathbf{r},t)$ is applied to the conductive medium with conductivity $\sigma(\mathbf{r})$ and we have the induced electrical field $\mathbf{E}(\mathbf{r},t)$ and current density $\mathbf{J}(\mathbf{r},t)$ in the medium. If the duration of the $\mathbf{B}_1(\mathbf{r},t)$ is short enough, the $\mathbf{E}(\mathbf{r},t)$ and $\mathbf{J}(\mathbf{r},t)$ can be written as $\mathbf{E}(\mathbf{r},t) \approx E(\mathbf{r})\delta(t)$, $\mathbf{J}(\mathbf{r},t) \approx \mathbf{J}(\mathbf{r})\delta(t)$, where $\delta(t)$ is the delta function. With static magnetic field $\mathbf{B}_0(\mathbf{r})$ and the corresponding Lorentz force $\mathbf{J}(\mathbf{r}) \times \mathbf{B}_0(\mathbf{r})$, a wave equation in the acoustically homogenous medium can be derived as[9]

$$\nabla^2 p(\mathbf{r}',t) - \frac{1}{c^2}\frac{\partial^2}{\partial t^2} p(\mathbf{r}',t) = \nabla \cdot [\mathbf{J}(\mathbf{r}) \times \mathbf{B}_0(\mathbf{r})] \cdot \delta(t), \quad (1)$$

where the $p(\mathbf{r}',t)$ is the acoustic pressure and c is the acoustic speed. The acoustic source distribution, i.e., the right hand side of Eq. (1) can be reconstructed using the time reversal method.[9,13] In practical experiments, an ultrasound transducer will act as a bandpass filter. The acoustic sources appearing at tissue interfaces corresponding to the conductivity discrepancy can be considered as wideband signals and will dominate in real ultrasound measurements.[10,11] Consequently, the reconstructed acoustic source map reflects the conductivity boundaries of the tissue, unless using a special method such as by multiexcitation.[14] The measured acoustic signal p_m can be estimated by Eq. (2)

$$p_m(\mathbf{r}',t) \propto \frac{1}{|\mathbf{r}-\mathbf{r}'|}\int_V d\mathbf{r}\{[\nabla\sigma(\mathbf{r})] \times \mathbf{E}(\mathbf{r})\} \cdot \mathbf{B}_0(\mathbf{r}). \quad (2)$$

In this study, in order to induce detectable MAT-MI signals in real human or animal tissue samples, we used a customized high-voltage coil driver to drive a coil embedded in a 2 mm thickness plastic cylinder. The charging voltage of the driver is adjustable from 0 to 24 kV. We estimated the induced electrical field by using a sensing coil with diameter of 30 mm. The sensing coil was placed on the surface of the plastic cylinder containing the magnetic coil. For charging voltage at 24 kV, the maximum induced voltage in the sensing coil was around 120 V. Consequently, the peak induced electrical field was estimated to be 1250 V/m. We also conducted a similar test in the previous MAT-MI system.[11] Figure 1 shows the induced voltage from these two systems. For better comparison, five different charging voltages, i.e., 8, 12, 16, 20, and 24 kV were set in the present coil driver. It is obvious that the present magnetic stimulator offers much stronger excitation than the previous stimulator. In our present experiment system, we have a 15 mm spatial gap

a)Author to whom correspondence should be addressed. Electronic mail: binhe@umn.edu.

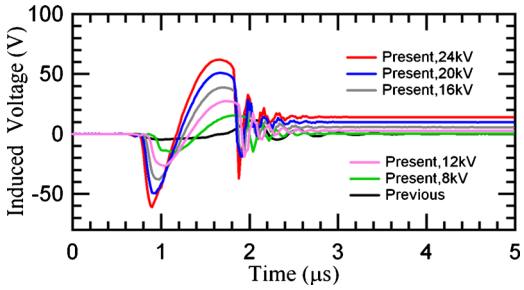

FIG. 1. (Color online) Comparison of the induced voltages in a sensing coil produced by the present MAT-MI system in comparison to previously reported MAT-MI system (see Ref. 11). Five different charging voltages in the present coil driver, i.e., 8, 12, 16, 20, and 24 kV were used for comparison.

between the sample and the stimulating coil. The induced electrical field applied to the sample was around 550 V/m which is comparable to the stimulating strength in transcranial magnetic stimulation (TMS).[15] However, the total energy applied to the samples in MAT-MI was much lower than TMS as MAT-MI pulse duration is at the microsecond level instead of hundreds of microsecond in TMS.

The MAT-MI system setup in the present study is similar to the previously reported system.[10,11] The transducer was mounted to a step motor to facilitate scanning in the XY plane. The unfocused 25 mm diameter transducer (TRS Ceramics) has a center frequency of 0.5 MHz, −6dB fractional bandwidth of 0.71. Two permanent magnets were placed on the top and under the bottom of the sample. The average magnetic flux density was 0.20 T. At each view angle, 2048 data points were recorded at a 5 MHz sampling rate.

Experiments on well-controlled saline-gel phantoms were first conducted. The phantom had a two layer structure as shown in Fig. 2(a). The outer layer and inner layer have diameters of 50 mm and 15 mm, respectively. The sample thickness was 25 mm. The outer layer was made with gel with 0.2% salinity to simulate healthy tissue with low conductivity. The inner layer was filled with a higher concentration saline solution to simulate cancerous tissue exhibiting high conductivity. Five different samples with salinity concentrations of 0.4%, 0.5%, 0.6%, 0.7%, and 0.8% were prepared for the inner layer. In ultrasound signal data collections, 100 times data averaging was adopted to improve the signal-to-noise ratio. After each test, direct conductivity measurements were conducted on the phantoms by four-electrode technique.[16] All electrodes had 300 μm diameter and were coated for electrical isolation, except for the 1.5 mm conductive. The separation of the adjacent electrode was 2 mm. Probe constant was obtained by measuring standard saline solution (Oakton) with a known conductivity of 0.86 S/m at the experimental temperature of 23 °C. The conductivity for 0.4%, 0.5%, 0.6%, 0.7%, and 0.8% salinity solutions were 0.74 S/m, 0.91 S/m, 1.06 S/m, 1.21 S/m, and 1.34 S/m, respectively. The outer gel had a conductivity of 0.40 S/m. All of these data were obtained at 0.5 MHz, similar to the center frequency of MAT-MI ultrasound signals. A photograph of the phantom was taken immediately after the experiments with the injection of blue ink into the inner layer for contrast enhancement. We reconstructed the images using the back-projection algorithm.[9] Figures 2(b)–2(f) depict the tomographic images with different conductivity contrasts ranging from 0.34 to 0.94 S/m. It can be seen that the reconstructed images are well consistent with the phantom geometry shown in Fig. 2(a). As shown in Fig. 2, the outer boundaries of the phantoms in the reconstructed MAT-MI images show almost the same image contrast as expected. Whereas the inner boundaries show increased image contrast as the target conductivity contrast increases.

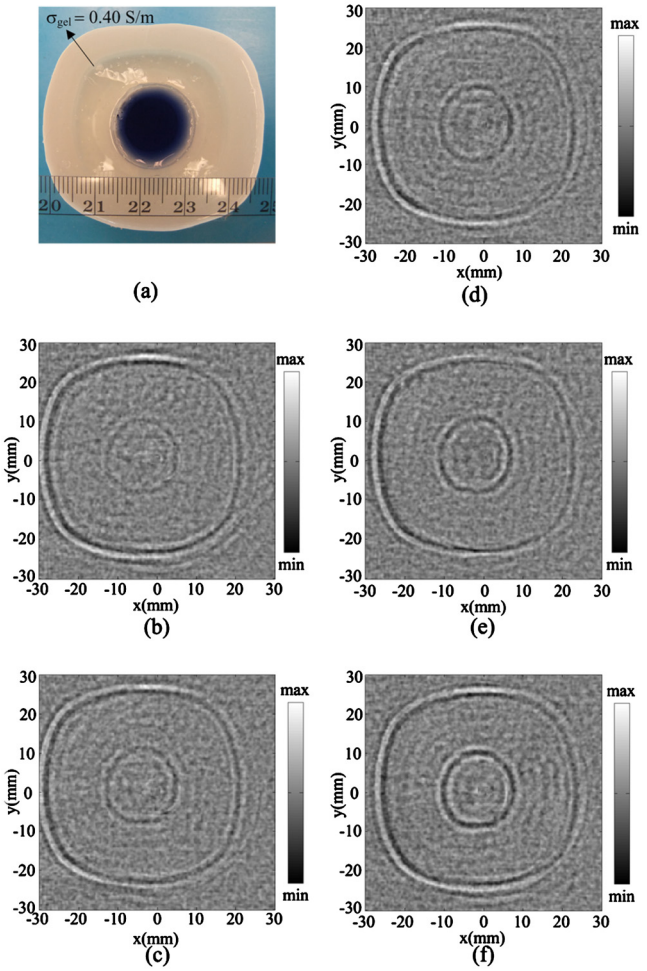

FIG. 2. (Color online) (a) Photograph of a double-layer saline phantom. The outer layer has 0.2% NaCl salinity with conductivity of 0.40 S/m. [(b)–(f)] Reconstructed MAT-MI images of phantoms with different inner layer conductivity of 0.74 S/m, 0.91 S/m, 1.06 S/m, 1.21 S/m, and 1.34 S/m, respectively.

We have also studied the imaging sensitivity at different magnetic stimulation strengths. Here, the contrast to noise ratio (CNR), defined as the ratio of the dynamic range of the reconstructed image to the standard deviation of the background noise, is used to evaluate the system sensitivity. In this study, single layer uniform phantoms with diameter of 50 mm, thickness of 25 mm, and different conductivities were placed in distilled water media which acts as a background with almost zero conductivity. Three different salinities, i.e., 0.3%, 0.5%, and 0.7% (corresponding to 0.52S/m, 0.91S/m, and 1.21S/m, respectively) and five different charging voltages, i.e., 8, 12, 16, 20, and 24 kV (corresponding to the stimulations in Fig. 1) are chosen. The testing results are illustrated in Fig. 3. We see better image contrast is obtained with the increase in the charging voltage/magnetic stimulation strength and conductivity contrast. This is consistent with our prediction in Eq. (2).

Real biological tissues generally have complex geometry, inhomogeneous conductivity distribution, and also attenuate ultrasound signals more significantly. We first used a

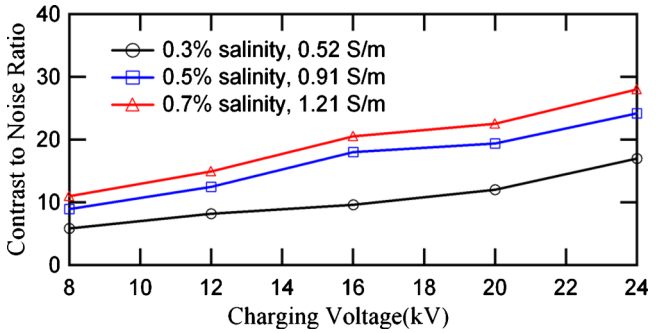

FIG. 3. (Color online) CNRs in the reconstructed MAT-MI images under different magnetic stimulation strengths and conductivity contrasts. Magnetic stimulations given by five charging voltages, i.e., 8, 12, 16, 20, and 24 kV were applied to a 50 mm diameter phantom with three conductivity contrasts, i.e., 0.52 S/m, 0.91 S/m, and 1.21 S/m.

sample of fresh pork to check imaging sensitivity. This sample retained the naturally formed fat-muscle-fat structure as shown in Fig. 4(a). The two outer fat portions had a width of 6 mm and the inner muscle portion had width of 3 mm. The size of the whole sample was 25 mm × 15 mm × 25 mm. The pork tissue was surrounded by gel with a salinity of 1.5%. Scanning of this phantom was done with an angular step of 2° and data averaging of 200 times at each view angle. In the conductivity measurements, the fat tissue exhibited very low conductivity around 0.02–0.03 S/m and no significant difference was found between the two fat portions. The muscle (in the longitudinal direction) showed much higher value ranging from 0.55 to 0.62 S/m. The gel

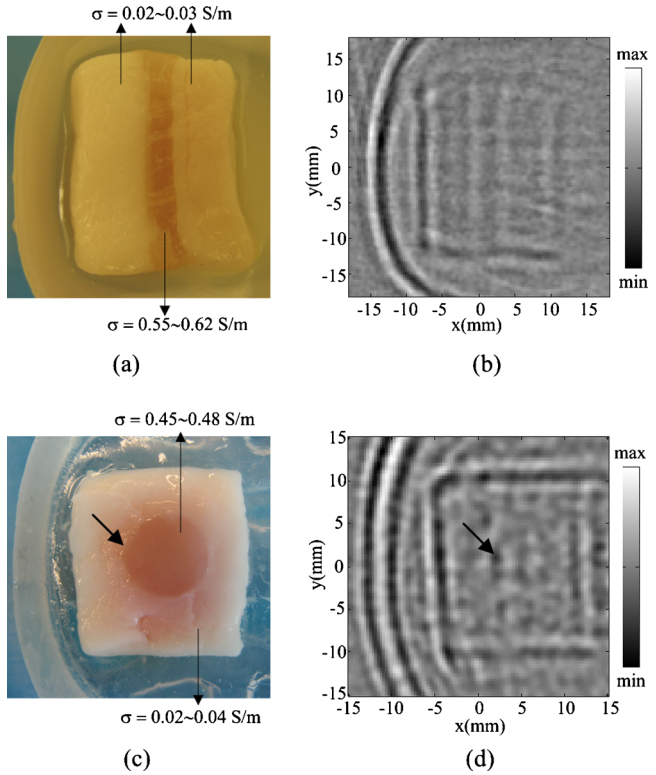

FIG. 4. (Color online) (a) Photograph of a fresh pork tissue sample. The muscle portion has 3 mm width. (b) Reconstructed MAT-MI image of the tissue sample shown in (a). (c) Photograph of a phantom made with turkey breast embedded in a piece of pork fat tissue. The turkey breast piece has a diameter of 6 mm. (d) Reconstructed MAT-MI image of the tissue sample shown in (c).

conductivity was 2.41S/m. Figure 4(b) shows the reconstructed MAT-MI image of the phantom. A good agreement can be observed between the reconstructed image and the phantom geometry shown in Fig. 4(a). The two inner vertical lines correspond to the two muscle-fat interfaces. The 3 mm spacing can be also distinguished. Figure 4(d) shows another imaging result from a tissue phantom shown in Fig. 4(c). In order to simulate abnormal tissue (e.g., tumor) surrounded by healthy tissues, the phantom was made by putting smashed turkey breast into a 6 mm diameter hole centered in a sample of pork fat tissue with a size of 20 mm × 16 mm × 10 mm. The conductivity of the turkey breast tissue was measured to be 0.46–0.48 S/m, and the conductivity of the pork fat tissue was 0.02–0.04 S/m. A digital bandpass filter was used in this experiment. From Fig. 4(d), we can still see the interface between the turkey breast and fat tissue as marked by the arrow. Compared to the pork phantom result, image quality is reduced because the sample is significantly thinner. Being that both the pork fat and turkey breast are soft tissues, it is difficult to build a perfect contact between these two tissue types in order to simulate the sharp tissue interfaces that usually exist in naturally formed tissue samples. In addition, we find that the conductivity interface between the turkey breast tissue and fat tissue is not very uniform along the Z direction, which may further deteriorate the signal quality.

In summary, we report that, using safe magnetic stimulation energy, the MAT-MI technique is capable of imaging real soft tissue with a conductivity contrast lower than 1.0 S/m, which suggests that the MAT-MI technique is sensitive enough for potential clinical applications.

The authors are grateful to Leo Mariappan for useful discussions on the phantom studies. This work was supported in part by NIH Grant No. R21EB006070, NSF Grant No. BES-0602957, NIH Grant Nos. RO1EB007920, RO1HL080093, and RO1EB006433.

[1]K. Paulson, W. Lionheart, and M. Pidcock, IEEE Trans. Med. Imaging **12**, 681 (1993).
[2]P. Metherall, D. C. Barber, R. H. Smallwood, and B. H. Brown, Nature **380**, 509 (1996).
[3]M. Joy, G. Scott, and M. Henkelman, Magn. Reson. Imaging **7**, 89 (1989).
[4]O. Kwon, E. Woo, J. Yoon, and J. K. Seo, IEEE Trans. Biomed. Eng. **49**, 160 (2002).
[5]A. J. Peyton, Z. Z. Yu, G. Lyon, S. Al-Zeibak, J. Ferreira, J. Velez, F. Linhares, A. R. Borges, H. L. Xiong, N. H. Saunders, and M. S. Beck, Meas. Sci. Technol. **7**, 261 (1996).
[6]B. C. Towe and M. R. Islam, IEEE Trans. Biomed. Eng. **35**, 892 (1988).
[7]B. J. Roth, P. J. Basser, and J. P. Jr Wikswo, IEEE Trans. Biomed. Eng. **41**, 723 (1994).
[8]H. Wen, J. Shah, and R. S. Balaban, IEEE Trans. Biomed. Eng. **45**, 119 (1998).
[9]Y. Xu and B. He, Phys. Med. Biol. **50**, 5175 (2005).
[10]X. Li, Y. Xu, and B. He, J. Appl. Phys. **99**, 066112 (2006).
[11]R. Xia, X. Li, and B. He, Appl. Phys. Lett. **91**, 083903 (2007).
[12]S. Gabriel, R. W. Lau, and C. Gabriel, Phys. Med. Biol. **41**, 2251 (1996).
[13]Y. Xu and L. H. V. Wang, Phys. Rev. Lett. **92**, 033902 (2004).
[14]X. Li and B. He, "Multi-Excitation Magnetoacoustic Tomography with Magnetic Induction for Bioimpedance Imaging," IEEE Trans. Med. Imaging (2010) (in press).
[15]V. Walsh and A. Cowey, Nat. Rev. Neurosci. **1**, 73 (2000).
[16]J. Z. Tsai, J. A. Will, S. Hubbard-Van Stelle, H. Cao, S. Tungjitkusolmun, Y. B. Choy, D. Haemmerich, V. R. Vorperian, and J. G. Webster, IEEE Trans. Biomed. Eng. **49**, 472 (2002).